The Involvement of Aryl hydrocarbon receptor in myelination and in human nerve sheath tumorigenesis

Ghjuvan Ghjacumu Shackleford, Nirmal Kumar Sampathkumar, Mehdi Hichor, Laure Weill, Delphine Meffre, Ludmila Juricek, Ingrid Laurendeau, Aline Chevallier, Nicolas Ortonne, Frédérique Larousserie, et al.

BIOLOGICAL SCIENCES: Neuroscience

The involvement of Aryl hydrocarbon receptor in myelination and in human nerve sheath tumorigenesis

Ghjuvan'Ghjacumu Shackleford*[1], Nirmal Kumar Sampathkumar*[1], Mehdi Hichor[1], Laure Weill[1], Delphine Meffre[1], Ludmila Juricek[1], Ingrid Laurendeau[2], Aline Chevallier[1], Nicolas Ortonne[3], Frédérique Larousserie[4], Marc Herbin[5], Ivan Bièche[2], Xavier Coumoul[1], Mathieu Beraneck[6], Etienne-Emile Baulieu[7], Frédéric Charbonnier[1], Eric Pasmant[2] and Charbel Massaad[1]

[1] University Paris Descartes, INSERM UMR 1124, Faculty of Basic and Biomedical Sciences, 45 rue des Saints-Pères, 75270, Paris Cedex 6, France

[2] EA7331, Faculté de Pharmacie de Paris, Université Paris Descartes, 4 avenue de l'Observatoire 75270 Paris Cedex 06, France

[3] Department of Pathology, Henri Mondor Hospital, 51, avenue de Lattre de Tassigny 94010, Créteil, France

[4] Department of Pathology, Cochin Hospital, 27 Rue du Faubourg Saint-Jacques, Paris, France

[5] CNRS UMR 7179, Muséum National d'Histoire Naturelle, Département Ecologie et Gestion de la Biodiversité, 57 rue Cuvier, 75231 Paris Cedex 05, France

[6] University Paris Descartes, CNRS UMR 8119, Faculty of Basic and Biomedical Sciences, 45 rue des Saints-Pères, 75270, Paris Cedex 6, France

[7] INSERM UMR-1195 and Paris-Saclay University, 94276 Le Kremlin-Bicêtre Cedex, France

Corresponding authors:

Pr Etienne-Emile Baulieu, INSERM UMR-1195 and Paris-Saclay University, 94276 Le Kremlin-Bicêtre Cedex, France. Phone: 33 1 49 59 18 82. email: etienne.baulieu@inserm.fr

Pr Charbel MASSAAD, University Paris Descartes, INSERM UMR 1124, 45 rue des Saints-Pères, 75270, Paris Cedex 6, France. Phone: 33 1 42 86 22 22. email: charbel.massaad@parisdescartes.fr

Keywords : AHR, Myelin, Nerve, MPNST, neurofibroma, Wnt/ beta catenin

Running title: AHR in Schwann cells.

ABSTRACT

Arylhydrocarbon receptor (*AHR*) is a ligand activated transcription factor involved in xenobiotic metabolism. Plexiform neurofibromas (PNF) can transform into malignant peripheral nerve sheath tumors (MPNSTs) that are resistant to existing therapies. These tumours are primarily composed of Schwann cells. In addition to *NF1* gene inactivation, further genetic lesions are required for malignant transformation. We have quantified the mRNAs expression levels of *AHR* and its associated genes in 38 human samples. We report that *AHR* and the biosynthetic enzymes of its endogenous ligand are overexpressed in human biopsies of PNF and MPNST. We also detect a strong nuclear AHR staining in MPNST. The inhibition of AHR by siRNA or antagonists, CH-223191 and trimethoxyflavone, induces apoptosis in human MPNST cells. Since AHR disregulation is observed in these tumors, we investigate AHR involvement in Schwann cell physiology. Hence, we studied the role of AHR in myelin structure and myelin genes regulation in $Ahr^{-/-}$ mice during myelin development. *Ahr* ablation leads to locomotion defects and provokes thinner myelin sheaths around the axons. We observe a disregulation of myelin genes expression, and myelin developmental markers in $Ahr^{-/-}$ mice. Interestingly, AHR does not directly bind to myelin gene promoters. The inhibition of AHR *in vitro* and *in vivo* increased β-Catenin levels and stimulated the binding of β-Catenin on myelin gene promoters. Taken together, our findings reveal a new endogenous role of AHR in peripheral myelination, and in peripheral nerve sheath tumors. Finally, we suggest a potential therapeutic approach by targeting AHR in nerve tumors.

Significance statement

Aryl hydrocarbon receptor (AHR) is well known to mediate xenobiotic metabolism in vertebrates. Growing evidences reveal that AHR seems to have endogenous roles in the development and functioning of different organs. In our current study, we describe a novel role of AHR in peripheral myelination and in nerve sheath tumours. We show that AHR pathway is disregulated in human biopsies of nerve tumours. The blockade of AHR provokes cell death in nerve tumours, suggesting a new therapeutic avenue in the treatment of this invasive cancer. Furthermore, the inhibition of AHR in mice provokes locomotor defects and

alteration of myelin structure. This work unravels a new endogenous role of AHR in peripheral myelination and a potential treatment of nerve tumours.

\body

INTRODUCTION

Neurofibromatosis type 1 (NF1, #MIM162200) is an autosomal dominant neuro-cutaneous tumor predisposition syndrome caused by germline heterozygous mutation in the *NF1* gene (1). The most common NF1-associated tumors are benign peripheral nerve sheath tumors called neurofibromas which may be dermal or plexiform (2). Dermal neurofibromas are typically small and grow as discrete lesions in the dermis whereas plexiform neurofibromas (PNF) can develop internally along the plexus of major peripheral nerves and become quite large. PNFs can undergo transformation to malignant peripheral nerve sheath tumors (MPNSTs) in about 10% of NF1 patients (3). MPNSTs are resistant to conventional therapies, and their deep-seated position and locally invasive growth hinder complete surgical resection with high degree of relapse rendering new treatments highly indispensable. Peripheral nerve Schwann cells (SCs) are the primary pathogenic cells in neurofibromas and MPNSTs, as bi-allelic mutation or loss of the *NF1* gene occurs uniquely in tumor SCs (4). *NF1* encodes the RAS-GAP (Rat sarcoma GTPase activating protein) neurofibromin, and RAS signaling is elevated in neurofibroma SCs (5). Neurofibromas may develop from SCs or Schwann cell progenitors (SCPs) due to the inactivation of *Nf1* at the SCP stage or in adult mice (6) (7).

Schwann cells (SC) carry out the myelination of axons in the nerve (8). Myelin is essential for rapid action potential propagation along the axons (9). Peripheral myelin genes expression (Myelin Protein Zero (P0) and Peripheral Myelin Protein-22 (PMP22)) is tightly regulated in SC (10). Krox20 (11), Wnt/β-Catenin signaling pathway (12) are known positive regulators of myelin gene expression, whereas Sox2 (13) and LXR (14) exert a negative effect.

Little is known of the additional cooperating genetic events potentially required for full plexiform neurofibroma's malignant transformation. Previous researches from our laboratory and others have shown an activation of the Wnt signaling pathway, during malignant transformation of plexiform neurofibromas to MPNSTs (15, 16). Indeed, Wnt pathway is a common conjuncture between myelin development as well and malignant transformation. There is a growing evidences that over-activation of AHR (aryl hydrocarbon receptor) signaling pathway can alter Wnt/β-Catenin signaling in development, different human cancers and disease (18, 19).

AHR is a ligand-activated transcription factor that is best known for mediating the toxicity and tumor-promoting properties of the carcinogen 2,3,7,8-tetrachlorodibenzo-p-dioxin (TCDD), commonly referred to as dioxin. The activation of AHR provokes its heterodimerisation with AHR Nuclear Translocator (ARNT). They bind specific responsive elements called Xenobiotic responsive elements (XREs), located in the promoter regions of the target genes and consequently, leading to their transactivation (e.g. Cytochrome 1A1). Nevertheless, its endogenous functions begin to emerge (17) and natural ligands of the AHR, like tryptophan derivatives, were identified. The AHR is present in ancient invertebrate organisms like *C. elegans*, where it is responsible for the regulation of GABAergic neuron fate specification (18). Kynurenine is a tryptophan catabolite generated *via* Tryptophan Dioxygenase (TDO) and Indoleamin 2,3-Dioxygenases (IDO). By activating AHR, kynurenine promotes tumor-cell survival and malignancy of glioma (19). Despite the discovery of the cognate ligand of AHR, the endogenous role of the AHR remains poorly explored, especially in the peripheral nervous system.

In this study, we report an upregulation of AHR signaling in PNF and MPNST. Furthermore, the inhibition of AHR promotes MPNST cell apoptosis. On the other hand, we investigate the role of AHR in normal Schwann cell physiology and myelin genes regulation using *Ahr-/-* mice. These mice have thinner myelin sheaths, dysregulated myelin genes expression, and consequent locomotor deficiencies. Taken together, our results elicit a novel role of the AHR in peripheral myelin genes regulation and a stimulation of AHR activity in malignant transformation of peripheral nerve sheath tumors. Our results also suggest that targeting AHR could be a promising avenue in the treatment of PNF and MPNST.

RESULTS

AHR signaling pathway is activated in peripheral nerve sheath tumorigenesis

In a series of 38 tumors, we first analyzed mRNA expression of *AHR*, *AHRR* (AHR Repressor), and *ARNT* (Table 1). *AHR* was significantly up-regulated in plexiform neurofibromas (7-fold) and in MPNSTs (9-fold), compared to the dermal neurofibromas. *AHRR* was significantly down-regulated in plexiform neurofibromas (3-fold) and MPNSTs (2-fold) compared to the dermal neurofibromas, while *ARNT* expression was not significantly altered in either the plexiform neurofibromas or the MPNSTs.

Several genes implicated in AHR pathway were also tested, including kynurenine metabolism (*IDO1, IDO2,* and *TDO2*), inflammation and immune pathways (*IL1ß, IL6, IL8, CXCL5,* and *CXCL6*), SC markers (*S100B*, and *P0*) and the proliferation (*MKI67*). *IDO1*, and *TDO2* (but not *IDO2*) were significantly up-regulated in plexiform neurofibromas and in MPNSTs. Concerning the inflammatory pathway: *IL1ß, IL6, IL8, CXCL5,* and *CXCL6* mRNA levels showed significant overexpression in plexiform neurofibromas and in MPNSTs, compared to the dermal neurofibromas (Table 1). It is noteworthy that AHR and the enzymes of its endogenous ligands are remarkably higher in MPNSTs than in PNFs. The proliferation-associated gene *MKI67* was overexpressed in the MPNSTs. SC-specific genes (*S100B*, *P0*) expression was shown to be significantly down-regulated in MPNSTs.

We also performed an immunostaining of AHR in MPNST (Fig. 1). We detected strong nuclear AHR staining in a proportion of tumor cells, while intra-tumoral vessels and fibroblasts in a fibrous septum (taken as internal negative controls) were not stained. Altogether, our data show that AHR pathway is activated in human PNFs and MPNSTs.

AHR inhibition induced apoptosis in MPNST cell lines.

As we observed AHR pathway is activated in human plexiform neurofibromas and MPNSTs. Subsequently, we hypothesized that inhibiting the AHR could affect MPNST cell survival. We used two AHR antagonists (CH and TMF) to inhibit AHR activity in STS26T. Treatment with CH-223191 (50μM at 48h and 72h) modestly increased cell death and enhanced apoptosis and shifted to late apoptotic state (Double positive for both Annexin and PI cell population) as quantified by Annexin V and PI staining (Fig.2A: 48 h, and Fig.2B: 72

h; Fig.S1A). CH did not have any effect at 10 µM, whereas TMF exhibited a more potent effect on MPNST cell death even at 10 µM. TMF (10µM, 48h or 72h) decreased cell viability by approximately 50%. After incubation with TMF (10µM, 72h), approximately 20% of the cells underwent apoptosis and 30% were late apoptotic. As expected, CH-223191 and TMF inhibited the expression of AHR target gene: *CYP1A1* (Fig. 2C). To confirm that this is due to AHR inhibition, we silenced *AHR* by si*AHR*. *AHR* silencing also induced apoptosis in STS26T dose dependently (Fig 2D). Silencing of *AHR* drastically decreased the mRNA levels of *AHR* and its target genes *CYP1A1* and *CYP1B1* (Fig. 2E). As the IL1*ß* expression was enhanced in plexiform neurofibromas and MPNSTs (Table 1), accordingly the inhibition of AHR either by siRNA or antagonists reduced *IL1ß* expression in STS26T cells (Fig. 2F).

We confirmed these results using another MPNST cell line, 90-8. As expected, CH inhibited the expression of the classical AHR target genes: *CYP1A1* and *CYP1B1* (Fig. S2A). Treatment with CH (50µM) increased the number of dead cells (Fig. S2B, SC) and enhanced apoptosis. We confirmed this result with si*AHR* (Fig S2D, S2E). Furthermore, it also reduced the expression of *IL1ß* (Fig. S2G).

Ahr ablation in mice caused locomotor defects and led to thinner myelin sheath.

Given the fact that PNF and MPNST is a complex tumor with different cells, we analyzed the expression of *AHR* and related components in different cells like Schwann cells, mast cells and endothelial cells. *AHR* mRNA is predominant in Schwann cells and may suggest its importance in Schwann cells physiology (Table 2). The observed activation of AHR pathway and the down-regulation of myelin gene (*P0)* and as well as *S100B* in plexiform neurofibromas and MPNSTs compelled us to investigate further the role of AHR in normal Schwann cells. Henceforth, we analyzed AHR expression in sciatic nerves and Schwann cells (Fig. 3A - C). AHR is expressed in the nerve (Fig.3A, C) and is localized in the nucleus of SC as well as the perinuclear compartment (Fig. 3B).

We analyzed the locomotor behavior of $Ahr^{-/-}$. We measured stride time using a motorized treadmill (Fig. 3D). No significant difference was observed with treadmill speed at 10 cm/s. However, when treadmill speed was increased at 16 cm/s, $Ahr^{-/-}$ mice showed slower stride than WT. At higher speed, $Ahr^{-/-}$ mice were not able to maintain the rhythm and therefore could not be tested.

Mice were then subjected to fixed speed rotarod protocol (14 rpm) for five consecutive days where the time to withstand the rotating rod was measured (Fig. 3E). The WT mice significantly improved their performance over days indicating an amelioration of their motor coordination, whereas the time latency of *Ahr*$^{-/-}$ mice remained constant. Indeed, WT mice were able to stay on the rotating bar on day 5 while *Ahr*$^{-/-}$ mice remained only. Our findings suggest that the *Ahr*$^{-/-}$ have impaired locomotion and motor coordination. Then, we performed the static rod test (Fig. 3G). All WT mice stayed 100s on the bar. In contrast, *Ahr*$^{-/-}$ mice were unsuccessful in staying (Fig. 3H). Finally, motor performance was evaluated using a dynamic rod test. The *Ahr*$^{-/-}$ mice were 3-times slower than the WT mice in crossing the rod (Fig. 3I). The *Ahr*$^{-/-}$ mice also exhibited more faults while crossing the rod (Fig 3I).

We studied myelin structure by electron microscopy. The myelin sheath of *Ahr*$^{-/-}$ mice was significantly thinner than controls (Fig.3J, 3K) and the axonal perimeter was higher in *Ahr*$^{-/-}$ mice compared to controls (Fig.3L). We plotted the g-ratios of sciatic nerve fibers as a function of their respective axonal perimeters (Fig.3M). We observed reduction in myelin thickness for all axon calibers, but smaller axons were more affected.

Western blot showed significant increase of P0 and PMP22 in *Ahr*$^{-/-}$ sciatic nerves (Fig.3N). Consistent with these results, the expression of the negative regulator of myelination, Sox2, was reduced by 40% in *Ahr*$^{-/-}$ mice (Fig.3N), while the expression of active β-Catenin was enhanced by 2-fold and total β-Catenin was decreased by 40%. Therefore, the ratio active β-Catenin over total β-Catenin is increased by 3.5-fold in in *Ahr*$^{-/-}$ mice suggesting an activation of the Wnt/β-Catenin pathway.

Ahr is involved in myelination during development

To determine when these myelin abnormalities arose, we analyzed the expression pattern of AHR during the myelination process at P7, P21 and in 8-weeks old mice and compared it to the expression of positive modulators of myelination process: Krox20 and β-Catenin. As depicted in figure 4A, AHR expression was at the highest level at P7 and then decreased at later time points to reach its lowest level in adult mice. Krox20 expression gradually increased during the myelination process to attain the highest level at P21 and, as

expected, dropped in adult animals. Finally, β-Catenin increased at P21, and then its expression was brought back to the same levels of P7 and at 8WO.

Taking account of this difference in AHR expression during development, we analyzed structure of myelin sheaths from sciatic nerves of P7 mice (Fig. 4B). We observed a mild disorganization of myelin sheaths in *Ahr*$^{-/-}$ mice without affecting the g-ratio (Fig. 4C) or axonal perimeter (Fig.4D). Nevertheless, *Ahr*$^{-/-}$ mice displayed fewer myelinated axons (28.88±1.18 for WT *vs* 20.88±1.23 for *Ahr*$^{-/-}$, Fig.4E). P0 (-50%) and PMP22 (-60%) protein expression was decreased in 7-days-old *Ahr*$^{-/-}$ mice (Fig.4F). To explore if myelin gene inhibition is due to a dysregulation in the expression of the major transcriptional regulators of SC myelination, we quantified the expression of Sox2, Krox20, total β-Catenin and active β-Catenin. The knockout of *Ahr* did not affect the expression of Sox2. However, we observed a decreased Krox20 expression (-60%) that was confirmed by IHC experiments. We observed a 25% reduction of the number of Krox20 positive cells in the sciatic nerves as suggested by DAPI staining (Fig.4G). Furthermore, WB analyses showed that active β-Catenin expression was diminished by 30% in *Ahr*$^{-/-}$ nerves (Fig. 4F). As the amount of total β-Catenin is increased in *Ahr*$^{-/-}$ mice (+35%), we observed a decrease of the ratio of active β-Catenin over total β-Catenin suggesting an impairment of the Wnt/β-Catenin pathway at P7 when *Ahr* is knocked out. At P21, electron microscopy images revealed that myelin sheaths are affected by the deletion of *Ahr* (Fig. 4H). The g-ratio was decreased designating thicker myelin sheaths around the axons of *Ahr*$^{-/-}$ mice (Fig. 4I). The axonal perimeter was reduced (Fig. 4J) while the numbers of myelinated were not affected in *Ahr*$^{-/-}$ mice (Fig. 4K).

At P21, P0 and PMP22 expression were stimulated by 2-fold in *Ahr*$^{-/-}$ mice. Sox2 expression was not still affected, while the expression of all the positive regulators was activated in *Ahr*$^{-/-}$ mice: Krox20 (+50%), total β-Catenin (+60%) and active β-Catenin (+35%) (Fig. 4L). Altogether, our data point-out a crucial and differential role of *Ahr* during myelination process and highlight that *Ahr* knockout leads to defects in myelin sheaths.

AHR regulates myelin gene expression in Schwann Cells

We transfected MSC80 cells with either non-targeting siRNA (NT) or si*Ahr*. First, the efficacy of the knock-down was evaluated by RT-qPCR (Fig. S3A) and western blot (Fig. S3B). In addition, we assessed the functional efficacy of the si*Ahr* on *Cyp1A1*- Luciferase

activity that was reduced drastically (-80%) (Fig. S3C). The knock-down of *Ahr* increased mRNA levels of P0 and PMP22 by 50% (Fig. 5A) and the promoter activity of P0 as well as PMP22 (Fig 5B). Taken together, the silencing of *Ahr* in SC line or its knockout in mice led to a disregulation of myelin gene expression.

Then, we examined the mechanism by which the AHR regulates myelin gene expression. We identified by MatInspector software four potential binding sites for AHR on the level of *P0* promoter and one putative AHR binding site on *Pmp22* promoter (Fig. 5C). Therefore, we tested the AHR binding on *P0* and *Pmp22* promoters by ChIP. As a positive control, we assayed the binding of the AHR on the level of its target gene: *Cyp1A1* promoter. As expected the AHR bound to *Cyp1A1* promoter (Fig. 5D). This binding was enhanced by 2-fold after treatment with TCDD (100nM; 1h). However, we did not detect AHR interaction with any of the putative binding sites identified on *Pmp22* (Fig. 5E) and P0 (Fig. 5F), even after the incubation of MSC80 with TCDD (loading control: Fig. S4A). These data showed that AHR does not seem to interact directly with myelin gene promoters.

The other possible mechanism of action of AHR is the cross-talk with another signaling pathway. We previously showed that activated Wnt/β-Catenin pathway enhances the expression of peripheral myelin genes (12). Furthermore, we demonstrated that the knocking-out *Ahr* in mice altered β-Catenin expression in the sciatic nerve (Fig. 3N). Therefore, we addressed the question whether the action of AHR is mediated by Wnt/β-Catenin pathway. After silencing *Ahr* in MSC80 cells, we observed a 50% increase in the protein levels of active β-Catenin and a 30% increase of total β-Catenin levels (Fig. 5G). Furthermore, to support the hypothesis, knock down of *Ahr* led to a significant stimulation of mRNA expression levels of Wnt signaling components*: Lrp6*, *Dvl2*, *Dvl3*, *Axin2* (Fig. 5H). Then, we assayed the functionality of the Wnt/β-Catenin pathway. The SuperTOP Flash-Luciferase construct, bearing several binding sites for TCF/LEF, was activated by 2.5-fold 48h after si*Ahr* (Fig. 5I). To assess how AHR modifies β-Catenin levels in MSC80 cells, we assumed that AHR is able to interact with β-Catenin and stimulates its degradation as described in intestine cancer cells (20). Immunoprecipitation of AHR indicated protein-protein interaction of β-Catenin and AHR in MSC80 cells (Fig. 5J).

Consequently, we hypothesized that the knock-down of *Ahr* increases the recruitment of β-Catenin with TCF/LEF complex on the level of myelin genes promoters. We localized LEF/TCF-β-Catenin binding sites on P0 and PMP22 promoters (12) (Fig. 5K). ChIP assays with β-Catenin antibodies showed that *Ahr* silencing increased the recruitment of β-Catenin on *P0* (Fig. 5L, loading control: Fig. S4B) and *Pmp22* promoters (Fig. 5M, Fig. S4B). Moreover, the binding of β-Catenin was also enhanced after *Ahr* silencing on the level of a Wnt target gene, *Axin2* (Fig. S4C). GAPDH was used as a negative control (Fig. S4D). Collectively, these data demonstrate that AHR exerts its effect on myelin genes through Wnt/β-Catenin pathway.

DISCUSSION

We reveal that AHR plays a crucial role in myelination process of the nerve and is overexpressed in nerve tumors. In a series of NF1-associated nerve sheath tumors we demonstrated that AHR signaling pathway is activated. We further analyzed other genes linked to the AHR and involved in tryptophan metabolism that lead to the synthesis of kynurenine, an endogenous ligand of AHR (19, 21, 22). The expression of two genes participating to the first steps of tryptophan metabolism, namely *IDO1* and *TDO2*, was significantly increased in plexiform neurofibromas and MPNSTs. *IDO1* and *TDO2* found to be remarkably increased in malignant form compared to the benign form of these tumors suggesting an increased AHR activity in the malignant transformation. The enzyme IDO1 mediates the first, rate-limiting, step in tryptophan metabolites to kynurenine, and is up-regulated under an inflammatory microenvironment (23). Through generation of downstream metabolites, IDO1 enzyme activity may affect immunity, including specific immunomodulatory or cytotoxic functions (21). It has been reported that L-kynurenine activates AHR (19), which positively regulates IDO1 expression in immune cells such as dendritic cells. Our observation showing a progressive up-regulation of *IDO1* and *TDO2* in plexiform neurofibromas (3-fold and 5-fold), and a further stimulation in MPNSTs (50-fold and 25-fold) suggests that kynurenine synthesis leading to AHR activation may play a role in peripheral nerve sheath tumor progression to malignancy.

In addition to the biallelic inactivation of the *NF1* gene, supplemental genetic lesions are necessary for malignant progression of plexiform neurofibromas. Alterations of additional genes (*CDKN2A/B, TP53, SUZ12, EED*) were detected in MPNSTs (3 24),. We have previously shown that Wnt/β-Catenin pathway was dysregulated in MPNSTs (25), and the present study reveals that AHR pathway is also activated in these tumors. Furthermore, we have described an elevation of Wnt5a (25) and *AHR* expression in MPNST tumours. Conversely, the knock-down of *AHR* in MPNST cells inhibits Wnt5a expression (not shown). Therefore, our data suggest a possible link between AHR and Wnt/β-Catenin pathways in MPNST.

Consequently, we inhibited AHR in MPNST cell lines to alter their survival. Both AHR antagonists (CH-223191 or TMF) and si*AHR* induced apoptosis of two MPNST cell

lines: 90-8 and STS26T. Again, this observation highlights the importance of AHR in SC malignancy in addition to *NF1*. Furthermore, AHR inhibition could down-regulate *IL1ß* that was elevated in MPNST tumors. Previous results suggested that AHR activation coupled with inflammatory signals can lead to synergistic induction of IL6 expression in tumor cells (26). We revealed a significant increase of *IL1ß*, *IL6*, *IL8*, *CXCL5*, and *CXCL6* mRNA levels in plexiform neurofibromas and MPNSTs. These results confirm previous *in vitro* findings showing that AHR activation may promote the induction of IL6, and IL8 (27, 28),), and highlight the implication of the AHR in the regulation of inflammation pathway (29).

Previous studies from our laboratory and other have shown that some signaling pathways that are involved in myelination process (Wnt/ β-Catenin, mTOR, ERK) ,ironically or unfortunately, are deregulated in MPNST (, , (30, 31), 32). Therefore, we then enquired about the endogenous role of AHR in normal Schwann cell physiology and peripheral nerve myelination. We revealed that AHR is expressed in SC and in the sciatic nerve. We then revealed that *Ahr*$^{-/-}$ mice present an alteration in locomotion. Additionally, electron microscopy analyses depicted thinner myelin sheaths. These data unveil the role of the AHR on SC myelinating functions. Prenatal exposure of TCDD in rats provoked a delay in oligodendrocyte differentiation and maturation (34). TCDD could also disrupt the functions of AHR to provoke neuropathies. In fact, rats intoxicated by TCDD showed severe defects in myelin structure of tibial and sciatic nerve and reduction in nerve conduction velocity (35, 36). Our results not only reinforce the endogenous role of AHR in normal myelination process, but also the mechanism by which it regulates myelination.

P0 and PMP22 myelin proteins are essential for an adequate structure of myelin sheath. Indeed, their disregulation or mutation is deleterious for myelin sheath structure, leading to peripheral neuropathies. *P0* expression was drastically down-regulated in MPNST, and the knockout of the *AHR* enhanced *P0* expression in Schwann cells. We showed that AHR predicted binding motifs in *P0* and *PMP22* promoters did not recruit AHR. We postulated that action of AHR is possibly mediated by β-Catenin because we observed an increase of β-Catenin binding on TCF/LEF binding sites of *P0* and *Pmp22* promoters after *Ahr* knock-down. We also showed that the KO of *Ahr* in mice activated Wnt signaling in SC. AHR has a dual function in regulating gene expression as a ligand-activated transcription factor, and as an E3 ubiquitin ligase. Kawajiri et al., showed that AHR E3 ubiquitin activity

has a role in β-Catenin degradation pathway that is independent of the APC system in intestine (20). We assume that the inhibition of AHR may reduce the degradation of β-Catenin, which is consistent with (i) the direct interaction that we have detected between AHR and β-Catenin proteins, and (ii) the β-Catenin increase observed after *Ahr* knock-down.

In conclusion, our findings unraveled that the AHR is involved in myelination process. This pathway is over-expressed in nerve tumors, which could also serve along with Wnt/β- Catenin pathway, as new markers for this specific type of cancer. As the inhibition of AHR induced apoptosis of MPNST cells, we can propose that this approach is further translatable. For instance, using either nanoparticles ((38) 39) or Adeno Associated Virus (AAV) (40) to deliver si*AHR* to induce apoptosis of these malignant cells could be suggested in adjuvant to existing chemotherapy with reduced doses. This approach can reduce the complications like chemotherapy-induced peripheral neuropathy (CIPN). So, our results indicate that AHR could represent a novel and a potential therapeutic target for this type of peripheral nerve sheath tumors that are poorly responsive to the existing chemotherapeutics.

MATERIALS AND METHODS

Animals

Ahr knock-out mice are a gift from Prof. Alvaro Puga (Cincinnati, USA). *Ahr*$^{-/-}$ mice and wild-type controls were maintained on a mixed strain background (C57BL/6j:RJ) and housed in a temperature-controlled room with a 12 hours light/dark cycle. All experiments were performed on age-matched male mice. Adults animals were fed *ad libitum* with water and Global-diet® 2016S from Harlan (Gannat, France). All aspects of animal care were approved by the Regional Ethic Committee (authorization CE2-04).

Treadmill test: forced locomotion

Adult males *Ahr*$^{-/-}$ (n=5) and control mice were acclimated to the testing room during 24 hours before each test. The forced locomotion of the mice was investigated using a commercial motorized treadmill. The speed of the treadmill was controlled by a tachymeter. After habituation session (speed = 6cm/s), mice were tested at a speed of 10 cm/s and 16cm/s the next day.

Rod test- Static paradigm

The same set of animals was subjected to both the treadmill test and rod test. The set up consisted of a rod of 9.5 mm diameter and 5 cm length. After a period of habituation, animals were securely placed on the rod. The ability of the animal to remain on the rod without falling was investigated for a maximum period of 100 seconds.

Rod test- Dynamic paradigm

Dark platform were setup at one end of the rod, where the mice were let for habituation for 10 minutes. Mice were primed to walk from a start point along a bar (70 cm long, 9.5 mm diameter) fixed 30 cm above the bench. Once the mice had succeeded in reaching the final destination several times by priming procedure, the test was recorded in three trials. We calculated the speed, and the number of faults.

Rotarod Test: forced paradigm

Balance and motor coordination was tested using a motorized rotarod LE8200 apparatus (Bioseb, France). Adult were placed mice on a rotating treadmill drum (3 cm diameter) and mice's latency to fall during the first 5 minutes of the trial was noted. The average time of fall for each trial was measured. Fixed speed Rotarod at 14 rpm for five consecutive days for WT mice has been performed *Ahr*$^{-/-}$ mice (n=5).

Transmission electron microscopy

Electron microscopy was done using fixed sciatic nerves following the protocol described previously (14). Electron microscopy images were used for calculating the g-ratio by ImageJ.

Patients and Samples

After clinical examination, the surgical removal of dermal neurofibromas was proposed in case of esthetical burden. Resection or removal of plexiform neurofibromas was described previously (25).

Expression of genes involved in the AhR signaling pathway in patients' samples

RT-qPCR has been carried out as described previously(25).

Immunohistochemistry

Human samples

Immunohistochemistry of patient samples has been carried out as described previously(41). Immunostaining of AHR (rabbit polyclonal antibody clone H211, Santa Cruz) was done at 3 µg/ml after heat antigen retrieval in pH 6.0 citrate buffer. In all samples, we checked the absence of staining in intra-tumoral vessels and fibroblasts as internal negative controls.

Mouse samples

Sciatic nerves were dissected and immersed in 4% paraformaldehyde and embedded in OCT Sections (10 µm) were cut using Cryostat. P0 (Aves labs inc.) antibody, AHR antibody (Enzo). Then the samples were incubated at room temperature for 1h30 with the appropriate secondary antibody (Alexa Fluor 488 donkey anti-mouse, Cy3-conjugated AffiniPure Donkey anti-Rabbit and Cy3-conjugated Affinity Pure Donkey anti-Chicken). Nuclei were

stained with Hoechst 33342 (Pierce Biotechnology). Sections were imaged using a confocal microscope (LSM510; Carl Zeiss).

Cell culture

The mouse SC line (MSC80) was maintained in Dulbecco's minimal essential medium (DMEM) supplemented with 10% decomplemented fetal calf serum (Hyclone-Perbio), 1% penicillin, 1% streptomycin (Gibco) and 1% Glutamine. All cultures were grown at 37°C in a humidified atmosphere of 5% CO2.

The MPNST-derived cell lines STS26T and 90-8 were maintained in advanced RPMI-1640 with 15% heat-inactivated FBS, 2.75‰ Bovine Pituitary Extract, 100U/ml penicillin, and 100µg/ml streptomycin (Invitrogen).

Plasmids and chemicals

p1646 (Cyp1A1-luc) was graciously provided by Dr A. Puga (Cincinnati, USA). siRNAs directed against *Ahr* were purchased from Qiagen (Lafayette, CO). The *Ahr* was targeted by four siRNAs recognizing four different regions of *Ahr* transcript. TCDD was purchased from LGC standards, CH-22319 and 6, 2′, 4′-trimethoxyflavone (TMF) from Sigma.

Transient transfections

MSC80 cells (2.5 x 10^5 cells/well) were grown in 6-well plates, transfected using Effecten reagents according to manufactures instructions (Qiagen) and luciferase activity was determined using the enzymatic method described previously (42). The β-galactosidase activity was used to normalize the transfection efficiency.

STS26T or 90-8 cells were transfected with either Non-Targetting siRNA (DHARMACON) or si*AHR* (DHARMACON) using RNAiMAX (Thermo fisher) according to the manufacturer's instruction.

Western Blot

WB assay was performed using standard techniques. Primary antibodies against P0 (and PMP22 were purchased from Abcam and Sigma respectively, β-Catenin from BD

Transduction, Active β-Catenin from Millipore, α-tubulin) from Sigma, SOX2 from Abcam, and AHR from Enzo life science (Biomol SA-210).

qPCR for MSC80

Total RNA from cultured MSC80 was extracted using TRIzol® Reagent (Invitrogen, France) according to manufacturer's instruction. qPCR was done as described previously(14). All results were normalized to the *26S* mRNA level and calculated using the ΔCt method. The primer sequences used in real time qPCR are listed in the primers table.

Chromatin Immunoprecipitation

MSC80 cells (10^7) fixed with 1% formaldehyde for 10 min. The cross linking was quenched with 0.125M glycine for 10 minutes. Fixed chromatin was then isolated and physically sheared by sonication to obtain DNA fragments of length of 300-600 base pairs. Immunoprecipitation is done using Protein A/G magnetic nanobeads (Dynabeads life technologies). The antibodies used in ChIP assays are: 5 µg of AHR-specific antibody (Biomol SA-210) 5 µg of β-Catenin (BD transduction # 610154), Histone H3 (Signaling #2650), 5 µg Rabbit IgG (Sigma I5006). RT-qPCRs were done as mentioned earlier with the primer pairs listed in primers' table. Then the percentage of input has been calculated as mentioned in (43).

Co-Immunoprecipitation

MSC80 cell lysates were pre-cleared with protein-A (Dynabeads® life technologies) and then the total protein was measured with BioRad RCDC. The lysate has been treated with DNAse to digest the genomic DNA. 3 µg of AHR antibody (BD transduction) is used to enrich AHR in 100 µg of total protein by using protein A Dynabeads (Rabbit IgG is used as negative control). Finally, the enriched protein samples were blotted with usual standard WB techniques with β-Catenin antibody (Biomol SA-210).

Flow cytometry analysis

STS26T or 90-8 cells cultured in 12-well plates were treated with AHR antagonists or DMSO. Cells undergoing apoptosis at the indicated time were identified using Annexin V-FITC apoptosis detection kit (Abcam ab14085), following the manufacturer's instruction. BD FACSCanto™II was used. A total of 10000 events were recorded at a light scatter to exclude debris and aggregate with a flow rate of less than 200 cells/second for each assay. The compensations and the settings were adjusted according to the assay. Data were analyzed using FlowJo Software.

Statistical analysis

Unless otherwise specified, means of treatment groups were compared with one-way analysis of variance (ANOVA). When the ANOVA showed that there were significant differences between the groups, Tukey's test was used to identify the sources of these differences. A p value of ≤ 0.05 was considered statistically significant. Two groups comparisons were performed by the Student test. As the mRNA levels did not fit a Gaussian distribution in human samples, (a) the mRNA levels in each subgroup of samples were expressed as their median values and ranges, rather than their mean values and coefficients of variation, and (b) comparison between the three types of nerve sheath tumors were assessed by using the non-parametric Kruskal Wallis H test. Differences were considered significant at confidence levels greater than 95% ($p < 0.05$).

ACKOWLEDGEMENTS:

This work was funded by INSERM, University Paris Descartes, the Agence National pour la Recherche (ANR) and the Agence Nationale de Sécurité Sanitaire de l'Alimentation, de l'Environnement et du travail (ANSES). GGS, NKS, MH, and AC received PhD fellowships from the French Ministry of Research (MNRT). LJ received a PhD fellowship from Region Ile de France. The authors greatly acknowledge Dr Alain Schmitt of the Cochin Imaging Facility, Jean-Maurice Petit of the Imaging Facility des Saints Pères and Stephanie Dupuy from the flow cytometry facility.

REFERENCES

1. Friedman JM (1999) Epidemiology of neurofibromatosis type 1. *Am J Med Genet* 89(1):1–6.

2. Sabbagh A, et al. (2009) Unravelling the genetic basis of variable clinical expression in neurofibromatosis 1. *Hum Mol Genet* 18(15):2768–2778.

3. Tucker T, Wolkenstein P, Revuz J, Zeller J, Friedman JM (2005) Association between benign and malignant peripheral nerve sheath tumors in NF1. *Neurology* 65(2):205–211.

4. Serra E, et al. (1997) Confirmation of a double-hit model for the NF1 gene in benign neurofibromas. *Am J Hum Genet* 61(3):512–9.

5. Cichowski K, Jacks T (2001) NF1 tumor suppressor gene function: narrowing the GAP. *Cell* 104(4):593–604.

6. Chen Z, et al. (2014) Cells of Origin in the Embryonic Nerve Roots for NF1-Associated Plexiform Neurofibroma. *Cancer Cell* 26(5):695–706.

7. Wu J, et al. (2008) Plexiform and Dermal Neurofibromas and Pigmentation Are Caused by Nf1 Loss in Desert Hedgehog-Expressing Cells. *Cancer Cell* 13(2):105–116.

8. Garbay B (2000) Myelin synthesis in the peripheral nervous system. *Prog Neurobiol* 61(3):267–304.

9. Nave K-A, Werner HB (2014) Myelination of the Nervous System: Mechanisms and Functions. *Annu Rev Cell Dev Biol* 30(1):503–533.

10. Niemann A, Berger P, Suter U (2006) Pathomechanisms of mutant proteins in Charcot-Marie-Tooth disease. *NeuroMolecular Med* 8(1–2):217–241.

11. Topilko P, et al. (1994) Krox-20 controls myelination in the peripheral nervous system. *Nature* 371(6500):796–799.

12. Tawk M, et al. (2011) Wnt/beta-catenin signaling is an essential and direct driver of myelin gene expression and myelinogenesis. *J Neurosci* 31(10):3729–42.

13. Le N, et al. (2005) Analysis of congenital hypomyelinating Egr2Lo/Lo nerves

identifies Sox2 as an inhibitor of Schwann cell differentiation and myelination. *Proc Natl Acad Sci U S A* 102(7):2596–601.

14. Makoukji J, et al. (2011) Interplay between LXR and Wnt/β-catenin signaling in the negative regulation of peripheral myelin genes by oxysterols. *J Neurosci* 31(26):9620–9.

15. Quintana FJ, et al. (2008) Control of T(reg) and T(H)17 cell differentiation by the aryl hydrocarbon receptor. *Nature* 453(7191):65–71.

16. Watson AL, et al. (2013) Canonical Wnt/β-catenin Signaling Drives Human Schwann Cell Transformation, Progression, and Tumor Maintenance. *Cancer Discov* 3(6):674–689.

17. Long X, et al. (2015) MMP-12-mediated by SARM-TRIF signaling pathway contributes to IFN-γ-independent airway inflammation and AHR post RSV infection in nude mice. *Respir Res* 16:11.

18. Huang X, Powell-Coffman JA, Jin Y (2004) The AHR-1 aryl hydrocarbon receptor and its co-factor the AHA-1 aryl hydrocarbon receptor nuclear translocator specify GABAergic neuron cell fate in C. elegans. *Development* 131(4):819–28.

19. Opitz CA, et al. (2011) of the human aryl hydrocarbon receptor. *Nature* 478(7368):1–7.

20. Kawajiri K, et al. (2009) Aryl hydrocarbon receptor suppresses intestinal carcinogenesis in ApcMin/+ mice with natural ligands. *Proc Natl Acad Sci U S A* 106(32):13481–6.

21. Mezrich JD, et al. (2010) An interaction between kynurenine and the aryl hydrocarbon receptor can generate regulatory T cells. *J Immunol* 185(6):3190–8.

22. Zhai L, et al. (2015) The role of IDO in brain tumor immunotherapy. *J Neurooncol* 123(3):395–403.

23. Litzenburger UM, et al. (2014) Constitutive IDO expression in human cancer is sustained by an autocrine signaling loop involving IL-6, STAT3 and the AHR. *Oncotarget* 5(4):1038–51.

24. Zhu Y, Ghosh P, Charnay P, Burns DK, Parada LF (2002) Neurofibromas in NF1: Schwann cell origin and role of tumor environment. *Science* 296(5569):920–2.

25. Luscan A, et al. (2014) The activation of the WNT signaling pathway is a Hallmark in neurofibromatosis type 1 tumorigenesis. *Clin Cancer Res* 20(2):358–71.

26. DiNatale BC, Schroeder JC, Francey LJ, Kusnadi A, Perdew GH (2010) Mechanistic insights into the events that lead to synergistic induction of interleukin 6 transcription upon activation of the aryl hydrocarbon receptor and inflammatory signaling. *J Biol Chem* 285(32):24388–97.

27. Kolasa E, Houlbert N, Balaguer P, Fardel O (2013) AhR- and NF-κB-dependent induction of interleukin-6 by co-exposure to the environmental contaminant benzanthracene and the cytokine tumor necrosis factor-α in human mammary MCF-7 cells. *Chem Biol Interact* 203(2):391–400.

28. Vogel CFA, et al. (2014) Cross-talk between aryl hydrocarbon receptor and the inflammatory response: a role for nuclear factor-κB. *J Biol Chem* 289(3):1866–75.

29. Hollingshead BD, Beischlag T V, Dinatale BC, Ramadoss P, Perdew GH (2008) Inflammatory signaling and aryl hydrocarbon receptor mediate synergistic induction of interleukin 6 in MCF-7 cells. *Cancer Res* 68(10):3609–17.

30. Murray IA, et al. (2010) Evidence for ligand-mediated selective modulation of aryl hydrocarbon receptor activity. *Mol Pharmacol* 77(2):247–54.

31. Azim K, Butt AM (2011) GSK3β negatively regulates oligodendrocyte differentiation and myelination in vivo. *Glia* 59(4):540–553.

32. Kendall JJ, et al. (2016) CK2 blockade causes MPNST cell apoptosis and promotes degradation of β-catenin. *Oncotarget* 7(33):53191–53203.

33. Brundage ME, et al. (2014) MAF mediates crosstalk between Ras-MAPK and mTOR signaling in NF1. *Oncogene* 33(49):5626–36.

34. Fernández M, et al. (2010) A single prenatal exposure to the endocrine disruptor 2,3,7,8-tetrachlorodibenzo-p-dioxin alters developmental myelination and remyelination potential in the rat brain. *J Neurochem* 115(4):897–909.

35. Grehl H, Grahmann F, Claus D, Neundörfer B (1993) Histologic evidence for a toxic polyneuropathy due to exposure to 2,3,7,8 - tetrachlorodibenzo-p-dioxin (TCDD) in rats. *Acta Neurol Scand* 88(5):354–357.

36. Grahmann F, Claus D, Grehl H, Neundörfer B (1993) Electrophysiologic evidence for a toxic polyneuropathy in rats after exposure to 2,3,7,8-tetrachlorodibenzo-p-dioxin (TCDD). *J Neurol Sci* 115(1):71–75.

37. Ali HM, et al. (2014) Effects of Silencing the *RET/PTC1* Oncogene in Papillary Thyroid Carcinoma by siRNA-Squalene Nanoparticles With and Without Fusogenic Companion GALA-Cholesterol. *Thyroid* 24(2):327–338.

38. Ali HM, et al. (2014) Effects of siRNA on RET/PTC3 junction oncogene in papillary thyroid carcinoma: from molecular and cellular studies to preclinical investigations. *PLoS One* 9(4):e95964.

39. Li B, Tang J, Hong Y, Thrasher JB (2014) AAV-based AR SiRNA constructs eradicate prostate cancer in nude mice. *Cancer Res* 68(9 Supplement). Available at: http://cancerres.aacrjournals.org/content/68/9_Supplement/1347 [Accessed May 22, 2017].

40. Luscan A, et al. (2014) The activation of the WNT signaling pathway is a Hallmark in neurofibromatosis type 1 tumorigenesis. *Clin Cancer Res* 20(2):358–71.

41. Massaad C, Garlatti M, Wilson EM, Cadepond F, Barouki R (2000) A natural sequence consisting of overlapping glucocorticoid-responsive elements mediates glucocorticoid, but not androgen, regulation of gene expression. *Biochem J* 350 Pt 1:123–129.

42. Frank SR, Schroeder M, Fernandez P, Taubert S, Amati B (2001) Binding of c-Myc to chromatin mediates mitogen-induced acetylation of histone H4 and gene activation. *Genes Dev* 15(16):2069–82.

Figure legends

Table 1: **AHR *pathway is dysregulated in nerve tumors. A,*** Total RNA was isolated from patients having dermal neurfibromas (n=8), Plexiform Neurofibromas (n=16), and MPNST (n=14). RT-qPCR were performed using primers recognizing specifically the genes indicated. Table indicates median [range] mRNA levels. mRNA levels were normalized such that the median value of the dermal neurofibromas was 1. Kruskal Wallis H test was used to compare MPNSTs vs plexiform neurofibromas vs dermal neurofibromas.

Table 2: **AHR *is predominantly expressed in Schwann cells compared to mast cells and endothelial cells. A,*** Total RNA was isolated from normal human tissues. Table indicates median [range] mRNA levels. mRNA amounts (calculated as described in Materials and Methods) were normalized by using the endogenous control TBP transcript.

Figure 1: **AHR *nuclear staining is detected in MPNST tissues.*** Formalin fixed, paraffin embedded human MPNST samples were stained with Hematoxylin-eosin-saffron (HES) and AHR was revealed by a specific antibody. A strong nuclear AhR staining was detected in a proportion of tumor cells while intra-tumoral vessels (arrows) and fibroblasts in a fibrous septa (*) were not stained, taken as internal negative controls. Peroxidase technique, diaminobenzidine chromogen, haematoxylin counterstain. Scale bar 100 µm.

Figure 2: ***AHR inhibition causes apoptosis in MPNST cell line. A- B,*** STS26T cells were treated with either AhR antagonists (CH-223191 or TMF) or DMSO (vehicle) during 48h ***(A)*** or 72h ***(B)***. Cells are stained with Annexin and PI to detect cell death by flow cytometry: living cell population (Annexin V^-/PI^-), apoptotic cells (Annexin V^+/PI^-), late apoptotic cells (Annexin V^+/PI^+) and dead cells (Annexin V^-/PI^+). Results represent the means +/- SEM of at least four independent experiments. *p<.05, **p<.01, by Bonferroni's *post hoc* tests after one-way ANOVA when compared to DMSO. ***C,*** STS26T cell line was treated with either AHR antagonists (CH-223191 or TMF) or DMSO (vehicle). 48h later, total RNA was extracted and RT-qPCR was performed using primers recognizing *CYP1A1 and TBP* to normalize the results. They represent the means +/- SEM of at least five independent experiments. *p<.05, ***p<0.001 by Student's t test when compared to DMSO. ***D,*** STS26T cells were transfected with either siAhR (10nM and 20nM) or NT; 72h after medium change,

cells were stained with Annexin and PI to detect cell death by flow cytometry: living cell population (Annexin V^-/PI^-), apoptotic cells (Annexin V^+/PI^-), late apoptotic cells (Annexin V^+/PI^+) and dead cells (Annexin V^-/PI^+). Results represent the means +/- SEM of at least four independent experiments. *p<.05, **p<.01, by Bonferroni's *post hoc* tests after one-way ANOVA when compared to control (NT). ***E***, Human STS26T cell line was transfected with si*AHR* (20nM) or NT; 72h later, total RNA was extracted and RT-qPCR were performed using primers to amplify *AHR,* , *CYP1A1,* and *CYP1B1*. Results were normalized to the *TBP* mRNA level and represent the means +/- SEM of at least five independent experiments. *p<.05, ***p<0.001 by Bonferroni's test when compared to control (NT). ***F,*** STS26T cells were reverse transfected with si*AHR* (20nM) or NT, or incubated with CH-223191 (50µM, 72h), TMF (10µM, 72h) or DMSO. Total RNA was extracted and RT-qPCR experiments were performed using primers recognizing *IL1ß* and *TBP* to normalize. Results represent the means +/- SEM of at least five independent experiments. *p<.05, ***p<0.001 by Student's t test when compared with control (NT).

Figure 3: ***Ahr ablation modifies myelin structure and locomotor behavior in adult mice.*** ***A*****,** Immunohistochemistry was performed on WT sciatic nerve to localize AhR (green) and P0 (red). The slides were imaged using confocal microscope. This experiment was repeated at least three times, and a typical experiment is presented here. Scale bar = 100 µm. ***B,*** Immunocytochemistry experiment was performed on MSC80 cells. AHR localization is highlighted in red; nuclei were stained with Hoechst (blue). This experiment was repeated at least three times, and a typical experiment is presented here. Scale bar = 10 µm. ***C,*** Western blot showing the expression of AhR in MSC80 cells and in sciatic nerve. ***D, Gait parameter:*** 8 weeks-old WT and $Ahr^{-/-}$ mice were placed on a treadmill at the speed of 10 cm/s and 16 cm/s. Stride time was measured. ***E, Rotarod test :*** 8 weeks-old WT and $Ahr^{-/-}$ mice were subjected to Rotarod test for five days. The time that mice could stay on the Rotarod was measured each day. At least 5 animals per group were tested. *p<0.05, ** p<0.01 Tukey's *post hoc* tests after one-way ANOVA when compared with control for each day of the experiment. ***F*****,** ***Rod test*****:** Eight weeks-old WT and $Ahr^{-/-}$ mice were placed on the rod to perform either static or dynamic rod tests. Representative pictures of the posture of the mice on the rod. The red arrowhead indicates right hind limb where $Ahr^{-/-}$ mouse slipped ***G***, ***Static rod test***: Measurement of the time that WT and $Ahr^{-/-}$ mice could stay without dropping from

the rod. The test was stopped when mice succeed to stay 100 seconds. ***H*, *Dynamic rod test.*** The average speed to cross the rod was measured (cm/s). ***I,*** The number of faults (slips) counted for either WT or *Ahr*$^{-/-}$. At least 5 animals per group were tested. *p<0.05, **p<0.01, ***p<0.001 by Student's t test when *Ahr*$^{-/-}$ were compared to WT mice. ***J,*** Sciatic nerves were isolated from either *WT* or *Ahr*$^{-/-}$ mice (8-weeks old). Then, ultrathin (50 –90 nm) cross-sections were prepared from Epon embedded nerves. Scale bar, 2µm. ***K,*** Myelin thickness was calculated by g-ratio determination and ***L,*** axonal perimeter was estimated using electronic microscopy pictures quantified by ImageJ software. At least five animals per genotype were used. ***M,*** g-ratios were plotted against axonal perimeter. ***N,*** Adult male *WT* or *Ahr*$^{-/-}$ mice were sacrificed, and then their sciatic nerves were dissected (at least n=6 per group). Total proteins were extracted, and western blots were performed using antibodies against P0, PMP22, SOX2, KROX20, β-Catenin, Active β-Catenin and α-tubulin (loading control). Figures represent a typical experiment. Western blots were quantified using ImageJ software. Black horizontal line between the lanes in the gels signifies a crop was made. Error bars indicate SEM *p<0.05, **p<0.01, ***p<0.001 by Student's t test when *Ahr*$^{-/-}$ were compared to control mice.

<u>Figure 4:</u> ***The KO of Ahr alters myelin ultrastructure, myelin proteins and myelination regulators during development. A,*** sciatic nerves from P7, P21 and 8 weeks-old mice were extracted and total protein was prepared. AHR, KROX20, β-catenin expression levels were determined by WB. α tubulin served as loading control. Figures represent a typical experiment. Ultrathin (50 –90 nm) cross-sections were prepared from epon embedded P7, and P21 sciatic nerves. ***B,*** Electron micrographs of P7 mice (scale bar = 2µm) ***C,*** Myelin thickness of P7 mice sciatic nerves was estimated by g-ratio determination using electron microscopy pictures quantified by Image J software. ***D,*** Axonal perimeter was measured by Image J software. ***E,*** The number of myelinated axons were counted in a given unit area***. F,*** P7 male WT or *Ahr*-/- mice were sacrificed, and then their sciatic nerves were dissected (at least n=6 per group). Total proteins were extracted, and western blots were performed using antibodies against P0, PMP22, Sox2, Krox20, β-Catenin, Active β-Catenin and α-tubulin (loading control). Figures represent a typical experiment. ***G,*** Immunohistochemistry was performed on WT or *Ahr*-/- sciatic nerves (P7). The slides were analyzed with a confocal

microscope: Krox20 (red), P0 (green), DAPI (blue). This experiment was performed with at least 4 animals per each group, and a typical experiment was presented here. Scale bars = 50 µm. The number of Krox20 positive cells and DAPI positive cells was counted by means of ImageJ. **$p<0.01$, by Student's **t**-test compared to control (WT). ***H,*** Electron micrographs of P21 mice (sale bare = 2µm), ***I***, g-ratio determination using electron microscopy pictures quantified by ImageJ software. ***J,*** Axonal perimeter was measured. ***K***, The number of myelinated axons were counted in a given unit area. Error bars indicate SEM. ***$p<0.001$, by Student's t test when *Ahr*-/- were compared to WT mice. ***L,*** P21 male WT or *Ahr*-/- mice were sacrificed, and then their sciatic nerves were dissected (at least n=6 per group). Total proteins were extracted, and western blots were performed using antibodies against P0, PMP22, Sox2, Krox20, β-Catenin, Active β-Catenin and α-tubulin.Figures represent a typical experiment. Western blots were quantified using ImageJ. Error bars indicate SEM *$p<0.05$, **$p<.001$, ***$p<0.001$, by Student's t test when *Ahr*-/- were compared to WT mice.

<u>Figure 5:</u> AHR *does not bind to myelin gene promoters in MSC80 cells but acts via Wnt/ß-Catenin pathway.* MSC80 cells were transfected with a siRNA directed against *Ahr* (si*Ahr*) or a non-targeting siRNA (NT). ***A***, Total mRNA was extracted and *P0* and *Pmp22* transcripts were quantified by RT-qPCR. All results were normalized to the 26S mRNA level. ***B,*** MSC80 cells were co-transfected with *siAhr* or *NT* and P0-luciferase or PMP22-luciferase constructs. Luciferase activity was assayed. Results represent the means +/- SEM of at least five independent experiments. *$p<.05$, ***$p<0.001$ by Student's t test when compared with control (NT). ***C.*** Putative binding sites of AHR located on the levels of P0 and PMP22 were identified by means of MatInspector software. MSC80 cells were incubated with vehicle (Nonane) or TCDD (100nM, 24h). Chromatin immunoprecipitation assays with antibodies against AHR or Mock IgG (non-relevant negative control) or Histone H3 (positive control) have been done. RT-qPCR was performed with primers recognizing AHR putative sites located on ***D,*** *Cyp1A1* an AHR target gene; ***E,*** *Pmp22;* ***F,*** *P0* genes. Results represent the means +/- SEM of at least four independent experiments. *$p<.05$, **$p<.01$, ***$p<0.001$ by Tukey's *post hoc* tests after one-way ANOVA when compared with control. MSC80 cells were transfected with siRNA directed against *Ahr (siAhr)* or a non-targeting siRNA (*NT*) for 48h. Proteins were extracted, and Western blots were performed using antibodies against ***G,***

Total β-Catenin or active β-Catenin and α-tubulin as a loading control. Figures represent a typical experiment. Western blots quantifications were done using ImageJ software. ***H,*** Total RNA was extracted, and quantitative real-time PCR experiments were performed using primers recognizing *Lrp6*, *Dvl2*, *Dvl3*, *Axin2*. RT-PCR was normalized using 26S RNA. Data represent the mean+/-SEM of at least four independent experiments. ***I,*** MSC80 cells were transiently transfected SuperTOP Flash-luciferase (STF-Luciferase) and with either *siAhr* or *NT*. 48h later, luciferase activity was analyzed. Results represent the means +/- SEM of at least six independent experiments performed in duplicate. *p<0.05, **p<0.01, by Student's t test. ***J,*** Co-immunoprecipitation assays were performed on MSC80 cells extracts using AhR, β -Catenin and IgG as a control. ***K,*** The binding sites for TCF/LEF- β-Catenin are localized on the promoter level for P0 and PMP22 as described by (12). MSC80 cells were transiently transfected with either si*Ahr* or NT for 48h after, Chromatin immunoprecipitation assays with antibodies against β-Catenin or Mock IgG or Histone H3 have been done. Primers recognizing TCF/LEF/β-Catenin binding sites on the levels of *P0 (**L**)*, *Pmp22 (**M**)* were used. Results represent the means +/- SEM of at four independent experiments. *p<.05, **p<.01, ***p<0.001 by Tukey's *post hoc* tests after one-way ANOVA when compared with control.

Figure S1: ***Representative dot plots of flow cytometry quantification***. ***A***, STS26T cells were treated either with AHR antagonists (CH (50µM) and TMF (10µM)) or Vehicle (DMSO) during 48h or 72h. Percentage of apoptotic cells (Annexin V^+/PI^-), dead cells (Annexin V^-/PI^+), late apoptotic cells (Annexin V^+/PI^+) and living cells (Annexin V^-/PI^-) was analyzed by flow cytometry. Human MPNST cell line (STS26T) was reverse transfected with either *siAHR* or *NT*. ***B,*** Representative dot plots of STS26T cells silenced with si*AHR*.

Figure S2: ***AHR inhibition causes apoptosis in MPNST cell line A,*** 90-8 cells were treated with either CH-223191 (50µM, 48h) or DMSO (vehicle). Total RNA was extracted and RT-qPCR experiments were performed using primers recognizing *CYP1A1* and *CYP1B1*. Results were normalized to the *TBP* mRNA level. They represent the means +/- SEM of at least five independent experiments. ***B-C*** 90.8 cells were treated with either CH-223191 (50µM, 48h or 72h) or DMSO (vehicle). 48h or 72 after treatment, cells are stained with Annexin and PI to detect cell death by flow cytometry: living cell population (Annexin V^-

/PI$^-$), apoptotic cells (Annexin V$^+$/PI), late apoptotic cells (Annexin V$^+$/PI$^+$) and dead cells (Annexin V$^-$/PI$^+$). Results represent the means +/- SEM of at least four independent experiments. *p<.05, **p<.01, by Bonferroni's *post hoc* tests after one-way ANOVA when compared to DMSO. ***D- E,*** MPNST cell line (90-8) was transfected with either NT or si*AHR*. 72 hours post medium change Annexin and PI staining were done. Percentages of apoptotic cells (Annexin V$^+$/PI$^-$), dead cells (Annexin V$^-$/PI$^+$), late apoptotic cells (Annexin V$^+$/PI$^+$) and living cells (Annexin V$^-$/PI$^-$) were analyzed by flow cytometry. ***F,*** Human 90-8 cell line was transfected with siAhR (20nM) or NT; 72h later, total RNA was extracted and RT-qPCR were performed using primers to amplify *AHR,* , *CYP1A1,* and *CYP1B1*. Results were normalized to the *TBP* mRNA level and represent the means +/- SEM of at least five independent experiments. *p<.05, by Bonferroni's test when compared to control (NT)..***G,*** 90-8 cells were treated with either AHR antagonists (CH-223191 50µM and TMF 10 µM) or DMSO (vehicle) and si*AHR*. Total RNA was extracted and RT-qPCR experiments were performed using primers recognizing *IL1ß*. Results were normalized to the *TBP* mRNA level. They represent the means +/- SEM of at least five independent experiments. *p<.05, ***p<0.001 by Student's t test when compared to control (NT).

Figure S3: ***Silencing efficiency of siAhr.*** MSC80 cells were transfected with non-targeting siRNA or a siRNA against *Ahr* (*siAhr*). ***A,*** Total RNA was extracted, and quantitative real-time PCR experiments were performed using primers recognizing *Ahr*. The RT-PCR was normalized using 26S RNA. Results represent the mean +/-SEM of at least eight independent experiments. ***B,*** Proteins were extracted and Western blots were performed using antibodies against AHR and α-tubulin (normalization of the Western blots). Figures represent a typical experiment. Western blots quantification was done using Image J software. The data represent the mean+/-SEM of at least 4 independent experiments. ***C,*** MSC80 cells were transiently transfected CYP1A1-luc construct and with either *siAhr* or *NT*. 48h later, luciferase activity was analyzed. Results represent the means +/- SEM of at least 6 independent experiments performed in duplicate. ***p<0.001 by Student's *t* test compared to control (NT).

Figure S4*: Controls for ChIP assays. A,* Western blot for ChIP assay where AHR antibody was used to precipitate AHR bound DNAs. MSC80 cells were treated with Nonane (vehicle)

or without TCDD for one hour and then fixed with PFA 4% to proceed with immunoprecipitation. ***B,*** Western blot for ChIP assay where β-Catenin antibody was used to precipitate β-Catenin - TCF/LEF bound DNAs. MSC80 cells were transfected with either non-targeting or *siAhr* for 48 hours and then fixed with PFA 4% to proceed with immunoprecipitation. ***C,*** Axin2 being a target gene of Wnt/β-Catenin served as a positive control. ***D,*** *Gapdh* served as a negative control.

Figure S5*: Uncropped western blots images of blots shown in main figures.*

Table 1. Median mRNA levels and ranges of 16 genes in dermal and PNFs and MPNSTs

	Dermal neurofibromas, $n = 8$		PNFs, $n = 16$		MPNSTs, $n = 14$		
Genes	Median	Range	Median	Range	Median	Range	P*
AHR pathway							
AHR	**1.00**	0.13–11.59	**6.84**	0.01–71.01	**8.98**	0.57–63.28	$P < 0.05$
AHRR	**1.00**	0.56–8.44	**0.39**	0.13–1.60	**0.49**	0.07–1.80	$P < 0.01$
ARNT	**1.00**	0.76–3.38	2.12	0.65–5.78	1.71	0.49–7.62	NS
Trp metabolism							
IDO1	**1.00**	0.04–10.75	**2.98**	0.11–41.54	**49.38**	1.59–681.64	$P < 0.01$
IDO2	**1.00**	0.21–6.74	0.60	0.07–5.06	0.65	0.01–18.21	NS
TDO2	**1.00**	0.05–101.38	**7.21**	0.25–77.62	**24.77**	0.86–2,931.70	$P < 0.01$
Myelin SCs							
S100B	**1.00**	0.64–1.73	**0.82**	0.10–4.49	**0.02**	0.01–2.54	$P < 0.01$
MPZ	**1.00**	0.10–1.79	**0.46**	0.10–2.54	**0.01**	0.01–2.24	$P < 0.01$
Inflammation							
IL-1B	**1.00**	0.26–4.09	**19.44**	0.01–809.67	**6.15**	2.66–644.12	$P < 0.05$
IL-6	**1.00**	0.50–1.95	**19.86**	0.18–247.60	**25.67**	3.06–32.04	$P < 0.05$
IL-8	**1.00**	0.07–3.15	**8.98**	0.01–648.32	**13.65**	0.19–269.89	$P < 0.05$
CXCL5	**1.00**	0.08–40.19	**32.42**	0.01–643.00	**185.53**	0.17–25,864.45	$P < 0.01$
CXCL6	**1.00**	0.01–5.66	**10.86**	2.28–1,642.39	**24.33**	4.60–862.02	$P < 0.01$
Xenobiotics metabolism							
CYP1A1	**1.00**	0.01–1.88	2.16	0.10–18.85	1.50	0.40–4.11	NS
CYP1B1	**1.00**	0.49–5.78	1.01	0.12–9.07	0.69	0.11–4.42	NS
Proliferation							
MKI67	**1.00**	0.30–2.82	**1.39**	0.88–4.77	**31.43**	13.6–82.9	$P < 0.01$

AHR pathway is dysregulated in nerve tumors. Total RNA was isolated from patients having dermal neurfibromas ($n = 8$), PNFs ($n = 16$), and MPNSTs ($n = 14$). qRT-PCR was performed using primers recognizing specifically the genes indicated. Table indicates median and range mRNA levels. mRNA levels were normalized such that the median value of the dermal neurofibromas was 1. Kruskal Wallis H test was used to compare MPNSTs vs. PNFs vs. dermal neurofibromas. NS, not significant. The bold values are statistically significant ($P < 0.05$). *Kruskal Wallis H test: MPNSTs vs. PNFs vs. dermal neurofibromas.

Table 2. Relative mRNA expression of eight genes in different human cells

Genes	SCs	Mast cells	Endothelial cell
AHR pathway			
AHR	426	11	6
AHRR	200	1,342	78
ARNT	1,105	492	479
Trp metabolism			
IDO1	10	NE	2
IDO2	NE	NE	NE
TDO2	14	3	NE
Myelin markers			
S100B	66,360	2	6
MPZ	24,336	4	5

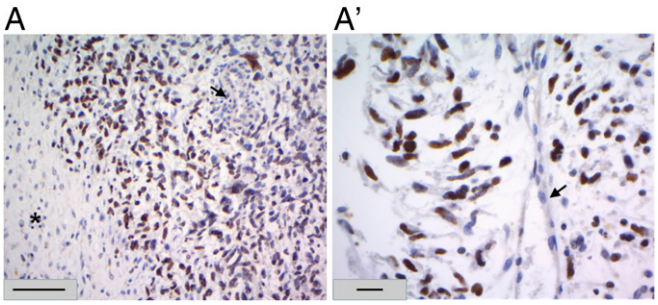

Figure 1.

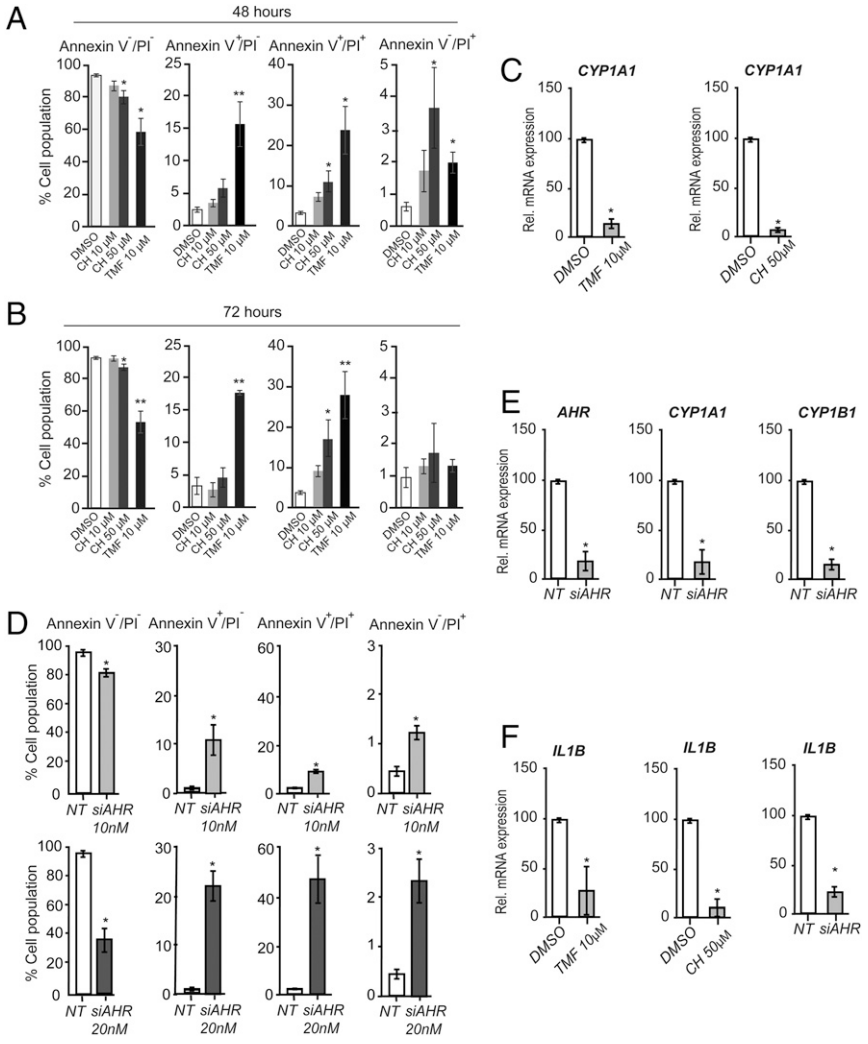
A
48 hours
Annexin V-/PI-
Annexin V+/PI-
Annexin V+/PI+
Annexin V-/PI+
% Cell population
DMSO
CH 10 µM
CH 50 µM
TMF 10 µM
B
72 hours
C
CYP1A1
Rel. mRNA expression
DMSO
TMF 10µM
CH 50µM
D
NT
siAHR
10nM
20nM
E
AHR
CYP1A1
CYP1B1
F
IL1B

Figure 2.

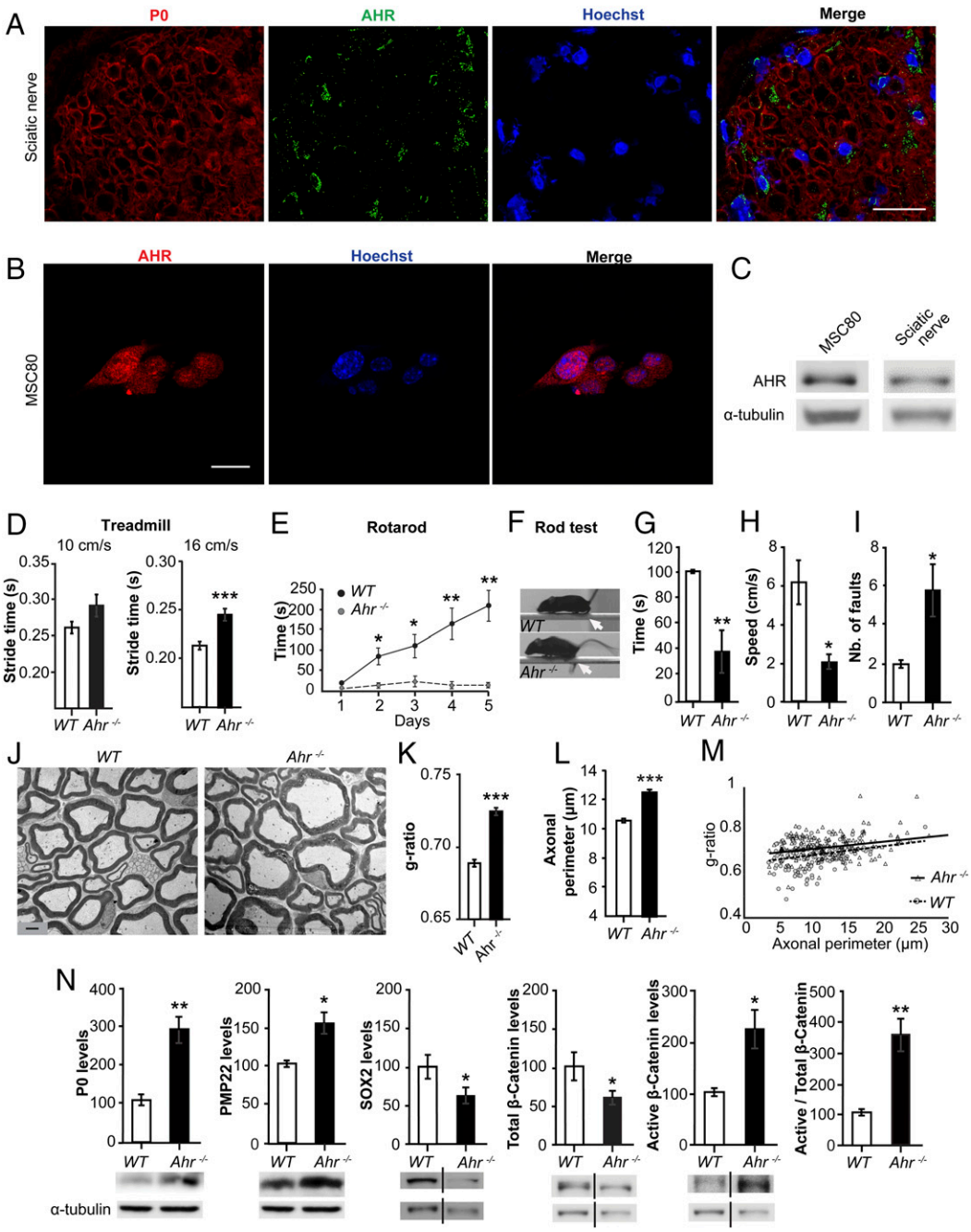
A
P0
AHR
Hoechst
Merge
Sciatic nerve
B
AHR
Hoechst
Merge
MSC80
C
MSC80
Sciatic nerve
AHR
α-tubulin
D
Treadmill
10 cm/s
16 cm/s
Stride time (s)
WT
Ahr -/-
E
Rotarod
Time (s)
WT
Ahr -/-
Days
F
Rod test
WT
Ahr -/-
G
Time (s)
H
Speed (cm/s)
I
Nb. of faults
J
WT
Ahr -/-
K
g-ratio
L
Axonal perimeter (µm)
M
g-ratio
Axonal perimeter (µm)
Ahr -/-
WT
N
P0 levels
PMP22 levels
SOX2 levels
Total β-Catenin levels
Active β-Catenin levels
Active / Total β-Catenin
α-tubulin

Figure 3.

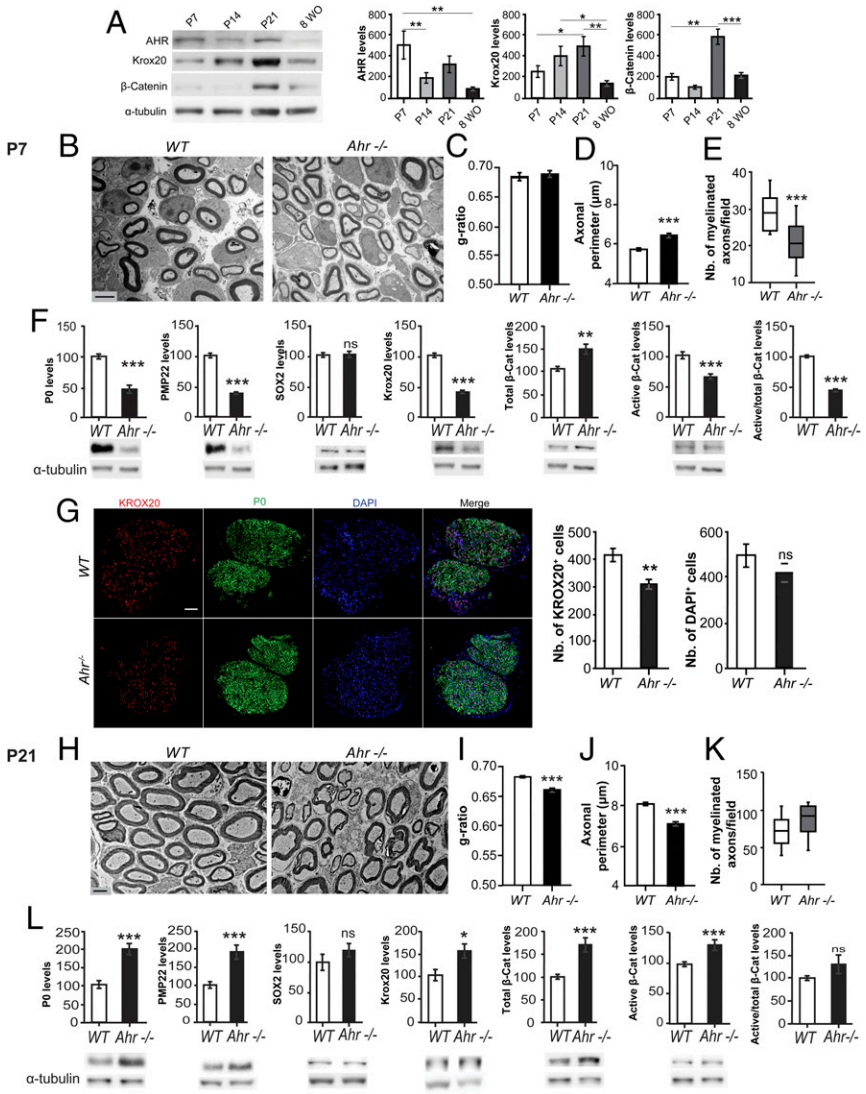
A
P7
P14
P21
8 WO
AHR
Krox20
β-Catenin
α-tubulin
AHR levels
Krox20 levels
β-Catenin levels
P7
P7
B
WT
Ahr -/-
C
g-ratio
D
Axonal perimeter (µm)
E
Nb. of myelinated axons/field
F
P0 levels
PMP22 levels
SOX2 levels
Krox20 levels
Total β-Cat levels
Active β-Cat levels
Active/total β-Cat levels
α-tubulin
G
KROX20
P0
DAPI
Merge
Nb. of KROX20+ cells
Nb. of DAPI+ cells
P21
H
I
J
K
L
ns

Figure 4.

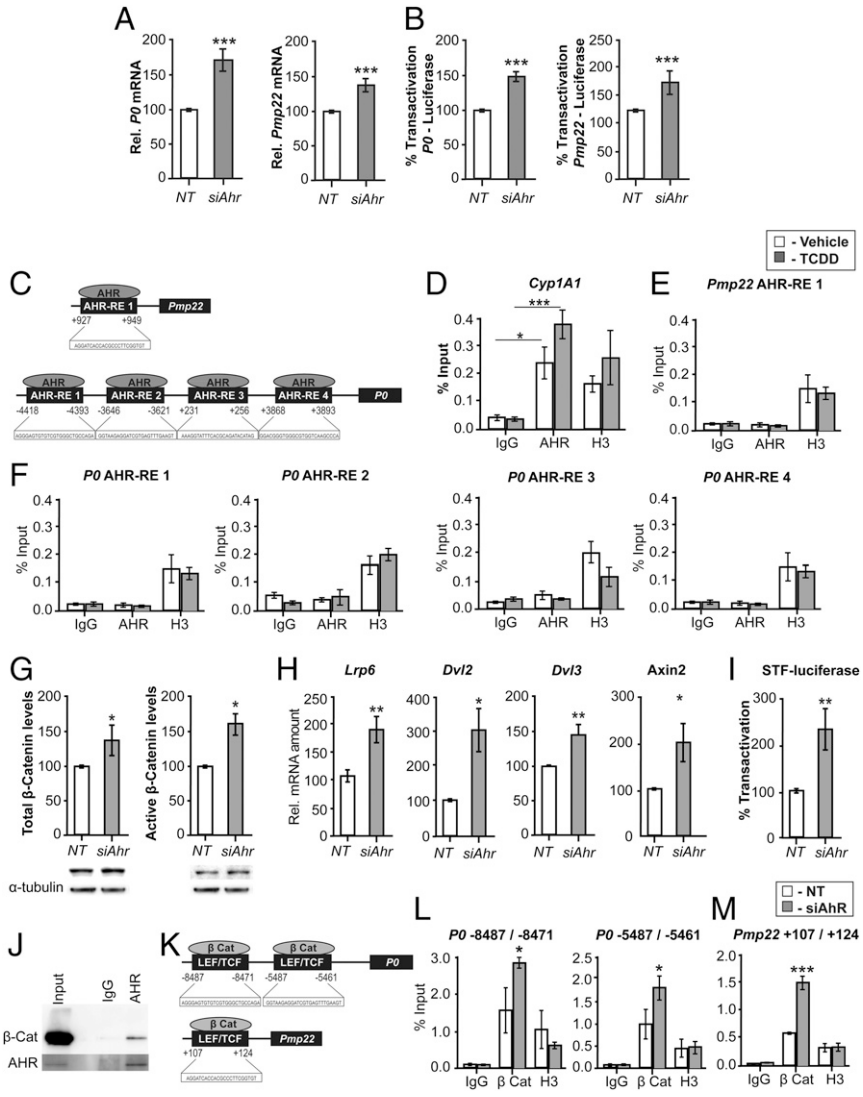
A
Rel. P0 mRNA
Rel. Pmp22 mRNA
NT
siAhr
B
% Transactivation P0 - Luciferase
% Transactivation Pmp22 - Luciferase
- Vehicle
- TCDD
C
AHR
AHR-RE 1
Pmp22
+927
+949
AHR-RE 2
AHR-RE 3
AHR-RE 4
P0
-4418
-4393
-3646
-3621
+231
+256
+3868
+3893
D
Cyp1A1
% Input
IgG
AHR
H3
E
Pmp22 AHR-RE 1
F
P0 AHR-RE 1
P0 AHR-RE 2
P0 AHR-RE 3
P0 AHR-RE 4
G
Total β-Catenin levels
Active β-Catenin levels
α-tubulin
H
Lrp6
Dvl2
Dvl3
Axin2
Rel. mRNA amount
I
STF-luciferase
% Transactivation
J
Input
IgG
AHR
β-Cat
AHR
K
β Cat
LEF/TCF
P0
Pmp22
-8487
-8471
-5487
-5461
+107
+124
L
P0 -8487 / -8471
P0 -5487 / -5461
β Cat
M
- NT
- siAhR
Pmp22 +107 / +124

Figure 5.

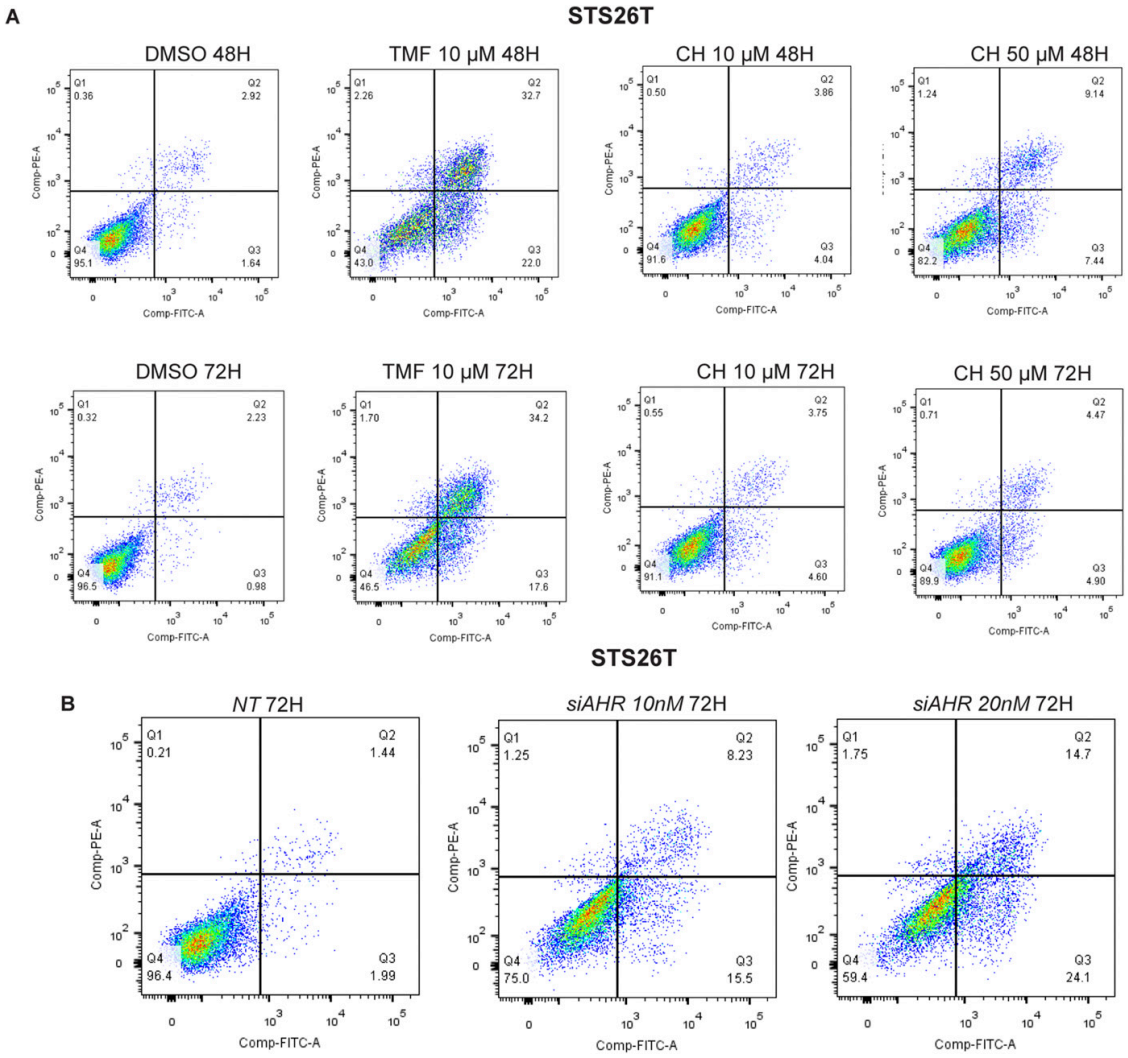
A
STS26T
DMSO 48H
TMF 10 μM 48H
CH 10 μM 48H
CH 50 μM 48H
DMSO 72H
TMF 10 μM 72H
CH 10 μM 72H
CH 50 μM 72H
Comp-PE-A
Comp-FITC-A
B
STS26T
NT 72H
siAHR 10nM 72H
siAHR 20nM 72H

Figure S1.

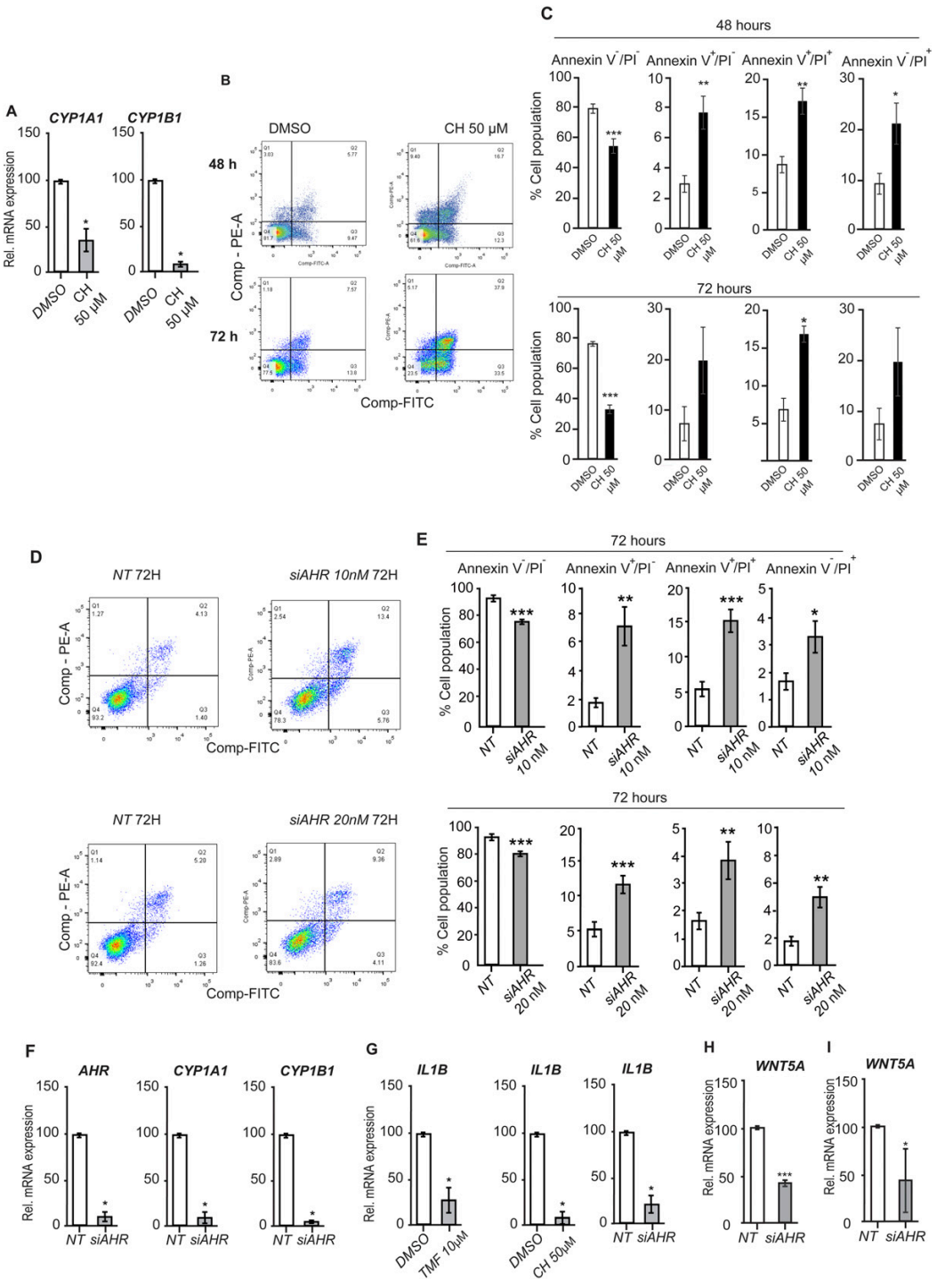
A
CYP1A1
CYP1B1
Rel. mRNA expression
DMSO
CH 50 µM
B
DMSO
CH 50 µM
48 h
72 h
Comp - PE-A
Comp-FITC
C
48 hours
72 hours
Annexin V-/PI-
Annexin V+/PI-
Annexin V+/PI+
Annexin V-/PI+
% Cell population
D
NT 72H
siAHR 10nM 72H
siAHR 20nM 72H
E
NT
siAHR 10 nM
siAHR 20 nM
F
AHR
CYP1A1
CYP1B1
NT siAHR
G
IL1B
DMSO
TMF 10µM
CH 50µM
H
WNT5A
I
WNT5A

Figure S2.

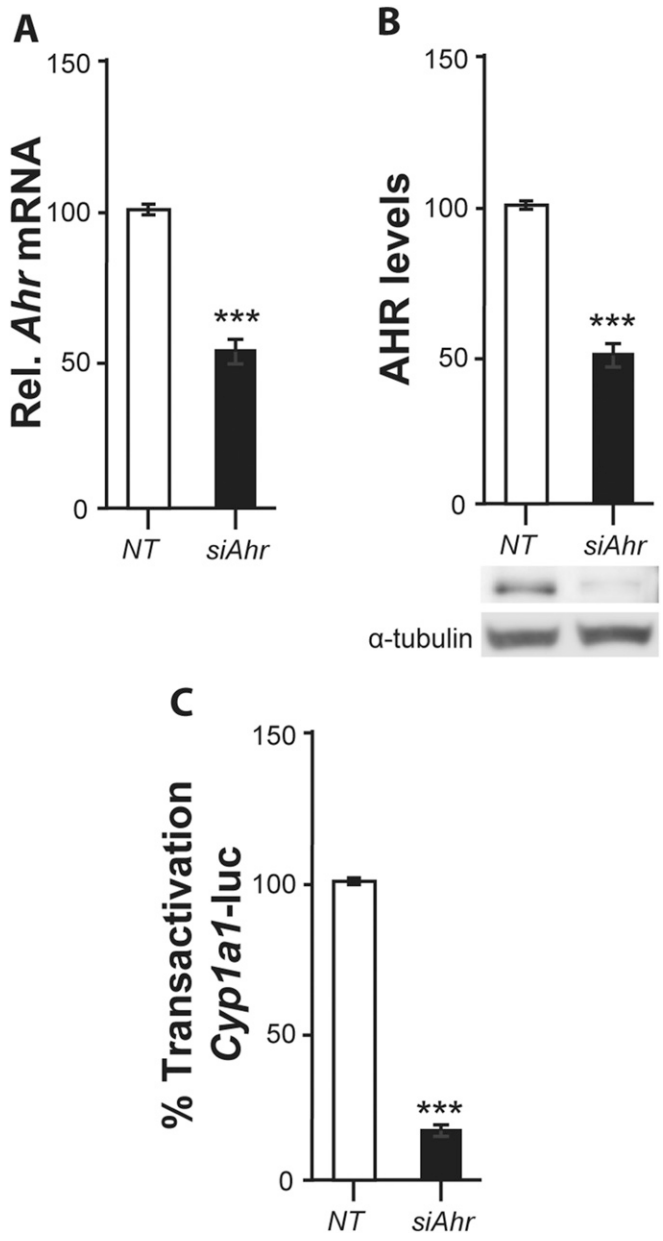
A
150
100
50
0
Rel. Ahr mRNA
***
NT
siAhr
B
150
100
50
0
AHR levels
***
NT
siAhr
α-tubulin
C
150
100
50
0
% Transactivation
Cyp1a1-luc
***
NT
siAhr

Figure S3.

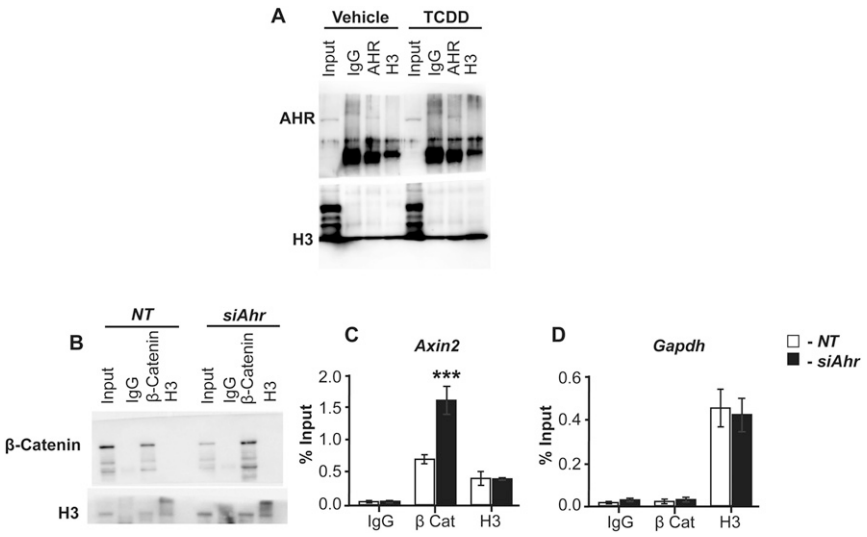
A
Vehicle
TCDD
Input
IgG
AHR
H3
AHR
H3
B
NT
siAhr
β-Catenin
H3
C
Axin2
***
% Input
IgG
β Cat
H3
D
Gapdh
- NT
- siAhr

Figure S4.

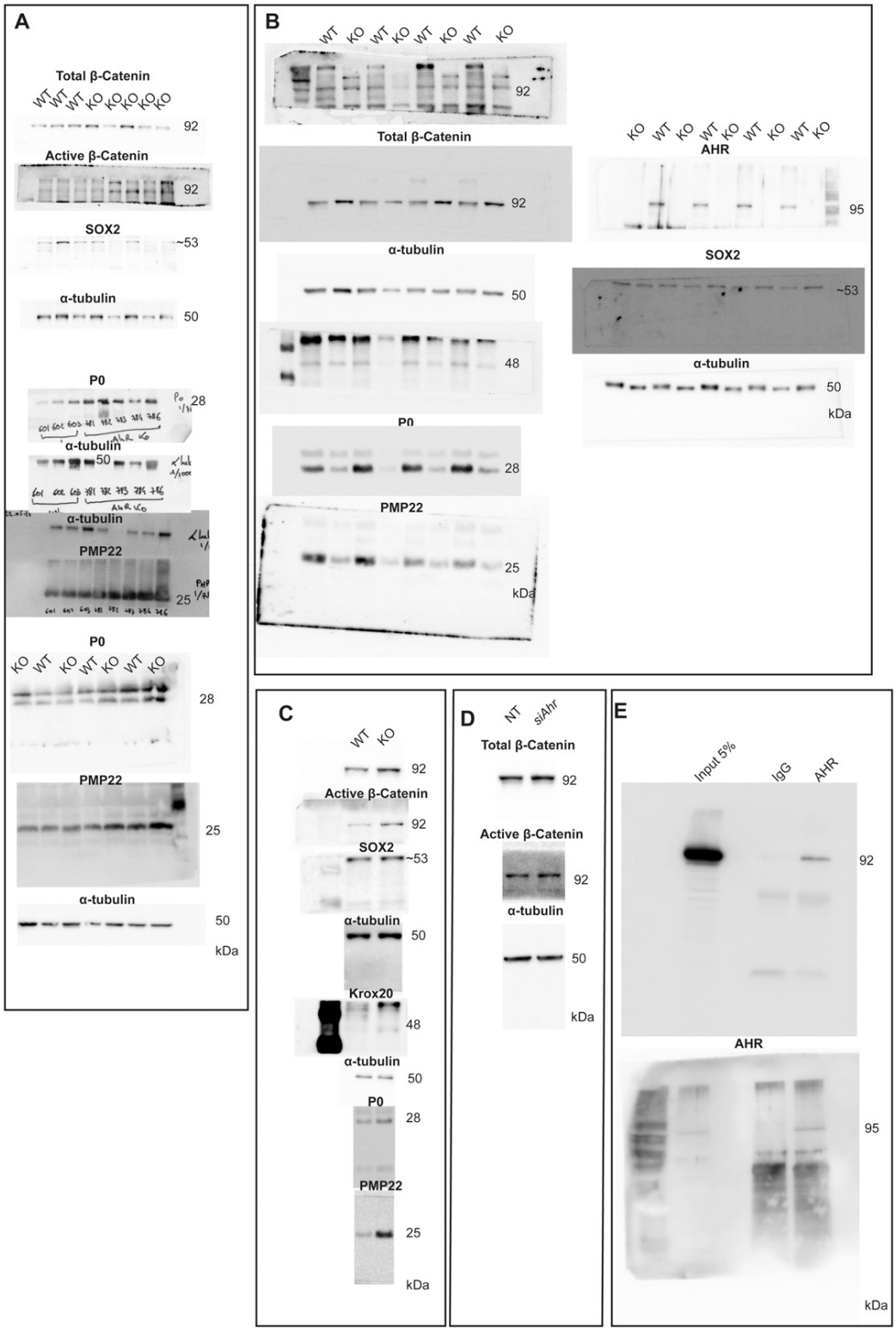
A
Total β-Catenin
WT WT WT KO KO KO KO KO
92
Active β-Catenin
92
SOX2
~53
α-tubulin
50
P0
28
α-tubulin
50
α-tubulin
PMP22
25
P0
KO WT KO WT KO WT KO
28
PMP22
25
α-tubulin
50
kDa
B
WT KO WT KO WT KO WT KO
92
Total β-Catenin
92
α-tubulin
50
48
P0
28
PMP22
25
kDa
KO WT KO WT KO WT KO WT KO
AHR
95
SOX2
~53
α-tubulin
50
kDa
C
WT KO
92
Active β-Catenin
92
SOX2
~53
α-tubulin
50
Krox20
48
α-tubulin
50
P0
28
PMP22
25
kDa
D
NT siAhr
Total β-Catenin
92
Active β-Catenin
92
α-tubulin
50
kDa
E
Input 5%
IgG
AHR
92
AHR
95
kDa

Figure S5

Table S1. List of primers used for RT-qPCR

Primers	Sequences
Ahr	F: 5′GCCTTGGTCTTCTATGCTCT3′
	R: 5′GCTTTGTGCTGGTTGTCAC3′
Dvl2	F: 5′GGCTTGTGTCGTCAGATACC3′
	R: 5′TTTCATGGCTGCTGGATAC3′
Dvl3	F: 5′CCGATGAGGATGATTCCACC3′
	R: 5′TGAGGCACTGCTCTGTTCTG3′
Axin2	F: 5′CCGATGAGGATGATTCCACC3′
	R: 5′TGAGGCACTGCTCTGTTCTG3′
Lrp6	F: 5′ACAGACACTGGCACGGATCG3′
	R: 5′GTTTGGCCAACCAAGGGAAG3′
26S	F 5′-AGGAGAAACAACGGTCGTGCCAAAA-3′
	R 5′-GCGCAAGCAGGTCTGAATCGTG-3′
RT-qPCR primers for β-catenin ChIP assays	
P0 (8487/8471)	F 5′-GGTCCTGAGTTCAAATCCC3-3′
	R 5′-GAACCTTCATCTGTTGTTGG-3′
P0 (5487/5461)	F 5′-TCTCTGGACAGAAAATGGAC-3′
	R 5′-TTAACTCCTGGCAATCCTG-3′
Pmp22 (-107/-124)	F 5′-GCTCCACCAGAGAACCTC-3′
	R 5′-TGCCAATCAAACTCACCAGAC-3′
GAPDH-promoter	F 5′-TCACCCTGCCCTCAATATCC-3′
	R 5′-TGTGCCTTTCATTCCATCCA-3′
Axin2-TSS′	F 5′-AAGGCCCTGCTGTAAAAGGT-3
	R 5′-GGGGGCTTTCTTTGAAGC-3′
Primers for clinical samples	
AHR-U	F 5′-TAA CCC AGA CCA GAT TCC TCC AGA-3′
AHR-L	R 5′-CCC TTG GAA ATT CAT TGC CAG A-3′
AHRR	F 5′-GGA AGG CTG CTG TTG GAG TCT CT-3′
AHRR-L	R5′-TGG AAG CCC AGA TAG TCC ACG A-3′
TBP-U	F5′-TGC ACA GGA GCC AAG AGT GAA-3′
TBP-L	R 5′-CAC ATC ACA GCT CCC CAC CA-3′

Primers that are not listed here will be provided on request.